PERGAMON

International Journal of Multiphase Flow 27 (2001) 415–435

International Journal of Multiphase Flow

www.elsevier.com/locate/ijmulflow

A model for non-suspension gas–solids flow of fine powders in pipes

David J. Mason[a,*], Avi Levy[b]

[a]*Department of Physical Sciences, Centre for Industrial Bulk Solids Handling, Glasgow Caledonian University, Cowcaddens Road, Glasgow, G4 OBA, UK*

[b]*Department of Mechanical Engineering, Ben-Gurion University of the Negev, Beer-Sheva, Israel*

Received 14 August 1999; received in revised form 6 April 2000

Abstract

The two-layer concept developed previously for a liquid–solids flow has been adapted to model *dense phase* transport of powders in pneumatic conveying systems. Many bulk materials of this type are capable of flowing in a non-suspension moving-bed type of flow. A new model for this type of flow in a horizontal pipe has been developed where the flow is modelled as two layers: a *dilute* gas–solids mixture flowing above a *dense* gas–solids mixture. For each layer, the conservation equations for mass, momentum and energy were solved for both the gas and solids phases. In addition, mass, momentum and energy transfers between the two layers were modelled. A single pressure was shared between the two layers. The paper describes the sub-models used to describe phenomena, such as the momentum transfer between the gas and solids in a layer. Transfer of mass, momentum and energy between the two layers results in a model that behaves in a similar manner to experimental observations. For example, as the mean flow velocity increases, the depth of the *dense* layer decreases. The predicted pressure profile for fully developed flow was compared with experimental data. In general, the prediction of pressure profile, and the predicted depth of the *dense* layer show reasonable agreement with the experimental observations. A parametric study was conducted to assess the relative significance of the initial conditions on the overall behaviour of the model. Variation of the initial conditions for the same total gas and solids mass flow rates was found to have only a small effect on the prediction of fully developed flow.

Keywords: Two-layer model; Stratify flow; Dense phase pneumatic conveying

* Corresponding author. Present address: School of Engineering, University of Brighton, Cockcroft Building, Brighton, BN2 4GJ, UK. Tel.: +44-1273-642-300; fax: +44-1273-642-301.

E-mail addresses: d.j.mason@brighton.ac.uk (D.J. Mason), avi@bgumail.bgu.ac.il (A. Levy).

0301-9322/01/$ - see front matter
PII: S0301-9322(00)00033-1

1. Introduction

The technique of transporting bulk particulate materials in pipes using a fluid is applied in many industrial processes. The conveying fluid may be either a liquid (hydraulic transport) or a gas (pneumatic transport). Seville et al. (1997) state that "at a mechanistic level, the distinction between hydraulic and pneumatic conveying lies in the ratio of the density of the conveyed solids to that of the conveying fluid". In a hydraulic conveying system, the density of the fluid is normally similar to that of the solids and the ratio of densities is constant. In a pneumatic conveying, the solids density is typically three orders of magnitude greater than that of the fluid and the ratio of densities changes along the pipe. As a result, the significance of particular flow phenomena is different in each type of system.

The effect of the density ratio can be seen in the number of particle wall collisions, which are reduced in hydraulic systems due to the magnitude of the lift force on the particles near the wall (Wilson et al., 1996). The change in the density ratio in pneumatic conveying systems results in a change in the transport velocity and, hence, the flow pattern, or even the mode of flow.

Dense phase pneumatic conveying systems have been applied in many industrial situations. These systems offer the potential benefits of lower energy consumption and reduced particle degradation, or pipeline wear. In such systems, the particles that comprise the bulk material are transported in a non-suspension mode of flow.

Many fine powders, such as cement and flour, which exhibit very low de-aeration rates, are suitable for *dense phase* transport. Observation of the flow patterns, in horizontal pipes, when these powders are transported in *dense phase* reveals a stratified flow. A high concentration layer of fluidised material occupies the lower portion of the pipe. In the upper portion of the pipe, particles are suspended in the transport gas.

In this paper, concepts developed to model the flow in hydraulic systems (Wilson, 1976) have been adapted and extended in order to describe the flow in a pneumatic system.

The pressure drop necessary to drive a particular combination of fluid and solids mass flow rates may be used to define the operating point of a conveying system. The operating envelope of a system is the set of all possible operating points that can be achieved by the particular combination of system and bulk material. For pneumatic conveying systems, this is commonly referred to as the conveying characteristic (Mills, 1990). The extent of the envelope is constrained by the characteristics of the components that comprise the system (for example, the maximum pressure rating of the air-mover, or pump), and the modes of flow that can be achieved by the material. The properties of the bulk material and the geometry of the pipeline govern the shape of the envelope (Mason et al. 1998a, 1998b).

1.1. Modes of flow

The results of many experimental studies have shown that gas–solids mixtures can flow in a wide variety of modes. Mason (1991) identified three basic modes of gas–solids flow in pipes, and classified materials according to their ability to achieve these modes of flow:

- *Dilute phase* flow only. Materials only capable of flowing when suspended in the conveying gas in a conventional pipeline (no flow conditioning along the pipeline).
- *Dense phase* moving-bed flow. Materials capable of a non-suspension mode of flow where the bulk material flows in a fluidised layer.
- *Dense phase* plug type flow. Materials capable of a non-suspension mode of flow where the bulk material flows in a series of full bore waves.

A bulk material that falls into any one of these groups can be conveyed in suspension if the conveying gas velocity is sufficiently high. With the two *dense phase* modes, flow is maintained at gas velocities below the saltation velocity in a horizontal pipe. For materials, which are only capable of being conveyed in *dilute phase*, the pipeline becomes blocked when the gas velocity falls below this critical value. Fargette (1998) and Jones et al. (1998) developed a method to identify modes of flow that could be achieved by bulk materials based upon the gas diffusion (permeability and de-aeration rate) and cohesive properties of the material. Materials that were capable of a *dense phase* mode of flow were not very cohesive and exhibited a permeability and de-aeration rate that were either both low (moving-bed flow) or both high (plug type flow).

This paper concerns the development of a model to predict the flow of bulk materials capable of the moving-bed type of *dense phase* flow. This is a mode of flow that can be achieved by a number of industrially important materials including cement, pulverised fuel ash (pfa), barytes, polyethylene powder and flour. Fig. 1 illustrates the modes of flow that can be achieved by such materials at various conveying gas velocities.

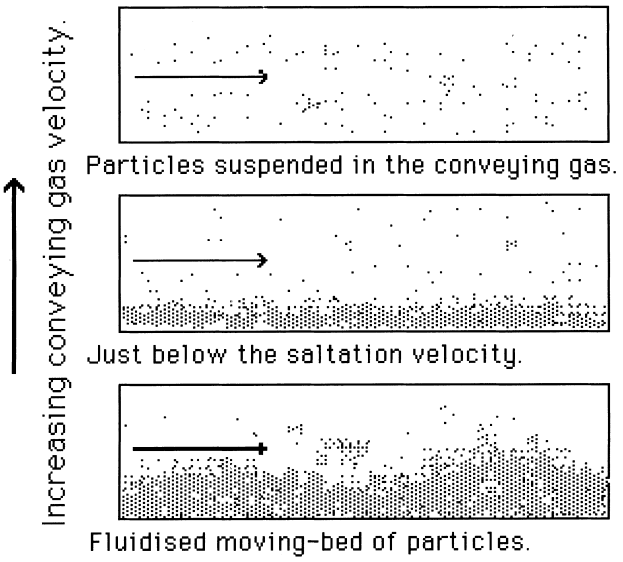

Fig. 1. Modes of flow achieved by materials capable of moving-bed type non-suspension flow.

1.2. Models

When a bulk material is transported through a horizontal pipe in the moving-bed mode of *dense phase* flow, two layers may be observed. The upper layer is a gas–solids mixture with a low solids concentration, while the lower layer is a gas–solids mixture with a high solids concentration. Similar types of stratified flow have been observed in liquid–solids flows.

In order to model this type of stratified liquid–solids flow, Wilson (1976) developed a two-layer model. This model is a one-dimensional model, which describes the flow of two layers in a pipe. The fluid–solids mixture in each layer is considered to be a single phase. Each layer has a separate velocity, with momentum transfer between the layers due to shear forces at their interface. This approach has been extended by a number of workers including Doron and Barnea (1993), who developed a three-layer model. In this case, the third layer is comprised of non-moving particles on the bottom of the pipe. With all these models, there is no mass transfer between the layers, and hence, the depth of each layer remains constant. For liquid–solids flows, this is not a significant limitation since the transport fluid is incompressible. For gas–solids flows, this is not the case, and experimental observations show a significant change in the depth of the layer as the transport fluid expands.

Another group of models developed to describe stratified gas–solids flow in pipes employs a force balance to compute the pressure drop. Bohnet (1965) developed the approach modelling the friction force in the *dilute* layer by an additional wall friction factor and that in the *dense* layer as Coulomb friction due to the weight of the layer. Muschelknaultz and Wojahn (1974) improved this by adding a shear force due to the interaction between the two layers. More recently, Hong and Tomita (1993) and Hong and Zhu (1997) refined this model by taking into account the nature of particle impacts on the *dense* layer and their subsequent settling or rebound.

2. Present study

A two-layer model for gas–solids flow in a straight horizontal pipe has been developed. The concept for the model was adapted from the two-layer model for hydraulic conveying developed by Wilson (1976). The geometric parameters used in the model are illustrated in Fig. 2. The height of the layer, h, can change due to mass transfer between the two layers.

In the subsequent discussion, the two layers are referred to as follows:

- The lower or *dense* layer, which has a higher solids concentration, is referred to as layer #1.
- The upper or *dispersed* layer, which has a lower solids concentration, is referred to as layer #2.

Mass transfer between the dense and the dispersed layers, #1 and #2 in Fig. 1, respectively, may occur in both directions. When the gas velocity in the top layer, #2, is larger than the saltation velocity, particles will be lifted from the bottom layer, #1, and join the dispersed phase in #2. When the gas velocity in #2 is below the saltation velocity, particles from #2 will settle onto the surface of the dense layer, #1. For the isothermal flow of a gas–solids mixture, the density of the gas phase decreases along the pipe due to the falling pressure. As a result,

the gas velocities in both layers must increase in order to satisfy the continuity law. As a consequence, mass is transferred from layer #1 to #2, and the height of the bottom layer decreases. This in turn causes a change in the cross-sectional area *seen* by each layer, which will also influence the gas velocities in both layers.

2.1. Geometric equations

The key feature of this mode of gas–solids flow is the height of the dense layer, #1. Thus, all the geometric parameters that influence the mass, momentum and energy transfer between the layers and other boundary conditions have been expressed in terms of this height. The cross-sectional areas and the perimeters, defined in Fig. 2, written as functions of the dense layer height are:

$$\tilde{S}_i = \frac{S_i}{D} = 2\left(\tilde{h} - \tilde{h}^2\right)^{1/2} \tag{1}$$

$$\tilde{S}_1 = \frac{S_1}{D} = \cos^{-1}(1 - 2\tilde{h}) \tag{2}$$

$$\tilde{S}_2 = \frac{S_2}{D} = \pi - \tilde{S}_1 \tag{3}$$

$$\tilde{A}_1 = \frac{A_1}{D^2} = \frac{1}{4}\left[\tilde{S}_1 - \tilde{S}_i(1 - 2\tilde{h})\right] \tag{4}$$

$$\tilde{A}_2 = \frac{A_2}{D^2} = \frac{\pi}{4} - \tilde{A}_1 \tag{5}$$

where

A_k is the area of the pipe cross-section occupied by layer k

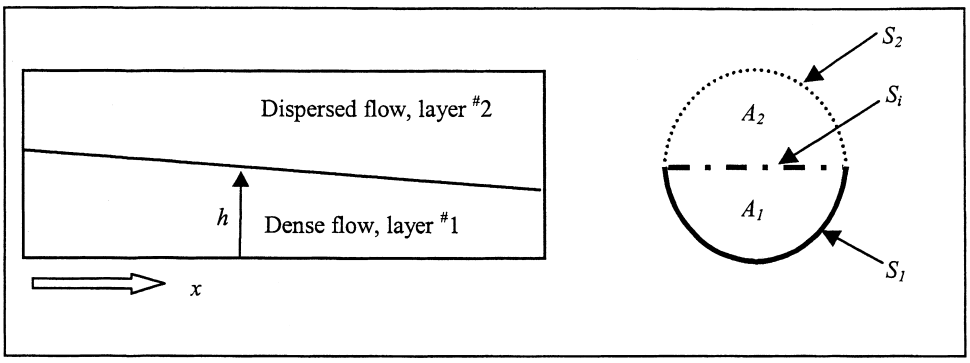

Fig. 2. The geometric parameters used in the model.

D is the pipe diameter
h is the height of the dense layer
$\tilde{h}$ is the non-dimensional dense layer height, $\tilde{h} \equiv h/D$
S_k is the 'wetted' perimeter of layer k
S_i is the length of the interface between the dense and the dilute layers

subscript $k = 1$ refers to the dense layer, and $k = 2$ refers to the dilute layer

From the definition of the volume fraction of a phase, for each layer:

$$r_{g1} + r_{s1} = 1 \tag{6}$$

$$r_{g2} + r_{s2} = 1 \tag{7}$$

where $r_{\alpha k}$ is the volume fraction of the phase α in layer k, subscript $\alpha = g$ refers to the gas phase, and $\alpha = s$ refers to the solids phase.

2.2. Balance equations

2.2.1. Mass balance equations for the gas and solids phases

$$\frac{d}{dx}\left(r_{g1}\rho_{g1}U_{g1}A_1\right) = S_{mg} \tag{8}$$

$$\frac{d}{dx}\left(r_{s1}\rho_{s}U_{s1}A_1\right) = S_{ms} \tag{9}$$

$$\frac{d}{dx}\left(r_{g2}\rho_{g2}U_{g2}A_2\right) = -S_{mg} \tag{10}$$

$$\frac{d}{dx}\left(r_{s2}\rho_{s}U_{s2}A_2\right) = -S_{ms} \tag{11}$$

where

$S_{m\alpha}$ is the mass transfer between the layers of the phase α
$U_{\alpha k}$ is the velocity of the phase α in layer k
x is the length in flow direction along the pipe
ρ_{gk} is the density of the gas phase in layer k
ρ_s is the density of the solids phase

The depth of the particles in the lower dense layer defines the interface between the two layers. Thus, when particles are lifted from the dense layer due to high velocities in the dilute layer, the height of the interface falls. This means that gas that was part of the dense layer is also transferred into the dilute layer. From a macroscopic point of view, mass transfer in this model has been considered as a transfer of gas–solids mixture between the dense and dilute layers.

Thus, a mass transfer from the dense layer to the dilute layer involves the transfer of particles and gas into the dilute layer and a corresponding reduction in the volume of the dense layer. In the present work, mass transfer due the pressure difference in a pipe cross-section was neglected.

2.2.2. Momentum balance equations for the gas and solids phases

$$\frac{\mathrm{d}}{\mathrm{d}x}\left(\rho_{\mathrm{g}1} r_{\mathrm{g}1} A_1 U_{\mathrm{g}1}^2\right) = S_{\mathrm{mg}} U_{\mathrm{g}1} - \tau_{\mathrm{g}1} r_{\mathrm{g}1} S_1 - r_{\mathrm{g}1} A_1 \frac{\mathrm{d}P_1}{\mathrm{d}x} - \rho_{\mathrm{g}1} r_{\mathrm{g}1} A_1 g \sin(\beta) - F_{\mathrm{d}1} \tag{12}$$

$$\frac{\mathrm{d}}{\mathrm{d}x}\left(\rho_{\mathrm{s}} r_{\mathrm{s}1} A_1 U_{\mathrm{s}1}^2\right) = S_{\mathrm{ms}} U_{\mathrm{s}1} - \tau_{\mathrm{s}1} r_{\mathrm{s}1} S_1 + (r_{\mathrm{g}2}\tau_{\mathrm{g}si} + r_{\mathrm{s}2}\tau_{\mathrm{s}si}) r_{\mathrm{s}1} S_i - r_{\mathrm{s}1} A_1 \frac{\mathrm{d}P_1}{\mathrm{d}x} - \rho_{\mathrm{s}} r_{\mathrm{s}1} A_1 g \sin(\beta) + F_{\mathrm{d}1} \tag{13}$$

$$\frac{\mathrm{d}}{\mathrm{d}x}\left(r_{\mathrm{g}2}\rho_{\mathrm{g}2} A_2 U_{\mathrm{g}2}^2\right) = -S_{\mathrm{mg}} U_{\mathrm{g}1} - \tau_{\mathrm{g}2} r_{\mathrm{g}2} S_2 - \tau_{\mathrm{g}si} r_{\mathrm{g}2} r_{\mathrm{s}1} S_i - r_{\mathrm{g}2} A_2 \frac{\mathrm{d}P_2}{\mathrm{d}x} - r_{\mathrm{g}2}\rho_{\mathrm{g}2} A_2 g \sin(\beta) - F_{\mathrm{d}2} \tag{14}$$

$$\frac{\mathrm{d}}{\mathrm{d}x}\left(r_{\mathrm{s}2}\rho_{\mathrm{s}} A_2 U_{\mathrm{s}2}^2\right) = -S_{\mathrm{ms}} U_{\mathrm{s}1} - \tau_{\mathrm{s}2} r_{\mathrm{s}2} S_2 - \tau_{\mathrm{s}si} r_{\mathrm{s}2} r_{\mathrm{s}1} S_i - r_{\mathrm{s}2} A_2 \frac{\mathrm{d}P_2}{\mathrm{d}x} - \rho_{\mathrm{s}} r_{\mathrm{s}2} A_2 g \sin(\beta) + F_{\mathrm{d}2} \tag{15}$$

where

$F_{\mathrm{d}k}$ is the inter-phase drag force between the phases in layer k
P_k is the gas phase pressure in layer k
β is the angle of inclination of the pipe axis above the horizontal
$\tau_{\alpha k}$ is the shear stress between the phase α and the pipe wall in layer k
$\tau_{\alpha si}$ is the shear stress between the phase α in layer #2 and the solids phase in layer #1

In writing Eqs. (12)–(15), it was assumed that:

- The friction force between the gas phase in layer #1 and the gas phase in layer #2 at the common interface S_i is negligibly small.
- The friction force between the gas phase in layer #1 and the solids phase in layer #2 at the common interface S_i is negligibly small.
- Forces due to gravity for pipes inclined at an angle β to the horizontal are taken into account.
- At the interface between the two layers, the contact surface is given by: $S_i = r_{sk} S_i + r_{gk} S_i$, where $r_{sk} S_i$ and $r_{gk} S_i$ are the contact surfaces with the interface for layer k for the solids and gas phases, respectively. This assumes that both phases in each layer are spread evenly on the inter-layer surface. Hence, the force that is acting between the solids phase in layer #1 and the solids phase in layer #2 transfers through the area $r_{\mathrm{s}2} r_{\mathrm{s}1} S_i$. Similarly, the force that is acting between the solids phase in layer #1 and the gas phase in layer #2 transfers through the area $r_{\mathrm{g}2} r_{\mathrm{s}1} S_i$.

2.2.3. Energy balance equations for the gas and solids phases

$$\frac{\mathrm{d}}{\mathrm{d}x}\left(r_{\mathrm{g}1}\rho_{\mathrm{g}1}U_{\mathrm{g}1}A_1\left(C_{\mathrm{pg}}T_{\mathrm{g}1}+\frac{U_{\mathrm{g}1}^2}{2}\right)\right)=S_{\mathrm{mg}}\left(C_{\mathrm{pg}}T_{\mathrm{g}1}+\frac{U_{\mathrm{g}1}^2}{2}\right)+Q_{\mathrm{g}1}-W_{\mathrm{g}1} \tag{16}$$

$$\frac{\mathrm{d}}{\mathrm{d}x}\left(r_{\mathrm{s}1}\rho_{\mathrm{s}}U_{\mathrm{s}1}A_1\left(C_{\mathrm{ps}}T_{\mathrm{s}1}+\frac{U_{\mathrm{s}1}^2}{2}\right)\right)=S_{\mathrm{mg}}\left(C_{\mathrm{ps}}T_{\mathrm{s}1}+\frac{U_{\mathrm{s}1}^2}{2}\right)+Q_{\mathrm{s}1}-W_{\mathrm{s}1} \tag{17}$$

$$\frac{\mathrm{d}}{\mathrm{d}x}\left(r_{\mathrm{g}2}\rho_{\mathrm{g}2}U_{\mathrm{g}2}A_2\left(C_{\mathrm{pg}}T_{\mathrm{g}2}+\frac{U_{\mathrm{g}2}^2}{2}\right)\right)=-S_{\mathrm{mg}}\left(C_{\mathrm{pg}}T_{\mathrm{g}1}+\frac{U_{\mathrm{g}1}^2}{2}\right)+Q_{\mathrm{g}2}-W_{\mathrm{g}2} \tag{18}$$

$$\frac{\mathrm{d}}{\mathrm{d}x}\left(r_{\mathrm{s}2}\rho_{\mathrm{s}}U_{\mathrm{s}2}A_2\left(C_{\mathrm{ps}}T_{\mathrm{s}2}+\frac{U_{\mathrm{s}2}^2}{2}\right)\right)=-S_{\mathrm{ms}}\left(C_{\mathrm{ps}}T_{\mathrm{s}1}+\frac{U_{\mathrm{s}1}^2}{2}\right)+Q_{\mathrm{s}2}-W_{\mathrm{s}2} \tag{19}$$

where

$C_{\mathrm{p}\alpha}$ is the specific heat capacity of the phase α at constant pressure
$T_{\alpha k}$ is the temperature of the phase α in layer k
$Q_{\alpha k}$ is the overall heat transfer for the phase α in layer k
$W_{\alpha k}$ is the overall work done by the phase α in layer k

For the case considered in this paper, the velocity contribution in the energy equations is small, and therefore, may be negligible from conservation point of view. Even so, it was decided to include these terms since they may be more significant in other applications of the model.

The heat transfer source terms, Q, in the energy equations for the gas and solids phases in each of the layers take into account heat transfer between:

- the gas and solid phases of the same layer;
- the gas phases in each layer;
- the gas phase of the top layer and the solid phase of the bottom layer
- the gas phases in each layer and the pipe wall.

In the course of this work, it was assumed that all the heat transferred from the pipe wall to each of the layers was transferred to the gas phase only. Hence, the overall heat transfer source terms for the above energy balance equation can be written as:

$$Q_{\mathrm{g}1}=Q_{\mathrm{g}1\leftrightarrow\mathrm{s}1}+Q_{\mathrm{g}1\leftrightarrow\mathrm{wall}}+Q_{\mathrm{g}2\leftrightarrow\mathrm{g}1} \tag{20}$$

$$Q_{\mathrm{s}1}=-Q_{\mathrm{g}1\leftrightarrow\mathrm{s}1}+Q_{\mathrm{g}2\leftrightarrow\mathrm{s}1} \tag{21}$$

$$Q_{\mathrm{g}2}=Q_{\mathrm{g}2\leftrightarrow\mathrm{s}2}+Q_{\mathrm{g}2\leftrightarrow\mathrm{wall}}-Q_{\mathrm{g}2\leftrightarrow\mathrm{g}1}-Q_{\mathrm{g}2\leftrightarrow\mathrm{s}1} \tag{22}$$

$$Q_{s2} = -Q_{g2\leftrightarrow s2} \tag{23}$$

where

$Q_{gk\leftrightarrow sk}$ is the heat transfer between the gas and solids phases in layer k
$Q_{gk\leftrightarrow wall}$ is the heat transfer between the gas phase and the pipe wall in layer k
$Q_{g2\leftrightarrow\alpha 1}$ heat transfer between the gas phase in layer #2 and the phase α in layer #1

The work terms, W, in the energy equations for the gas and solids phases in each layer take into account the work done by:

- the drag force between the gas and solid phases in each layer;
- the gravity force due to pipe inclination;
- the friction force between the two layers.

As a consequence, the work terms in the energy balance equation can be written as:

$$W_{g1} = -F_{d1}U_{s1} - r_{g1}\rho_{g1}U_{g1}A_1\sin(\beta) \tag{24}$$

$$W_{s1} = (\tau_{gsi} + \tau_{ssi})r_{s1}S_iU_{s1} + F_{d1}U_{s1} - r_{s1}\rho_sU_{s1}A_1\sin(\beta) \tag{25}$$

$$W_{g2} = -F_{d2}U_{s2} - \tau_{gsi}r_{s1}S_iU_{s1} - r_{g2}\rho_{g2}U_{g2}A_2\sin(\beta) \tag{26}$$

$$W_{s2} = F_{d2}U_{s2} - \tau_{ssi}r_{s1}S_iU_{s1} - r_{s2}\rho_sU_{s2}A_2g\sin(\beta) \tag{27}$$

2.2.4. Complimentary equations

In order to solve the above balance equations, some complimentary equations are required for: mass transfer, friction forces, equations of state, inter-phase drag forces, and heat transfer.

2.2.4.1. Mass transfer. The mass transfer source terms for both the gas and solids phases, S_{mg} and S_{ms}, respectively, have been calculated from the mass flow of the phase through the area change caused by the change in the height of the dense layer.

$$S_{mg} = \frac{1}{2}r_{g1}\rho_{g1}U_{g1}S_i\frac{dh}{dx} \tag{28}$$

$$S_{ms} = \frac{1}{2}r_{s1}\rho_sU_{s1}S_i\frac{dh}{dx} \tag{29}$$

2.2.4.2. Friction forces. The friction forces per unit length for a phase were calculated by multiplying the friction area per unit length (i.e. the relevant perimeter) by the shear stress between the phase and the layer boundaries (i.e. the pipe wall and the interface between the layers). The shear stress was calculated as a function of the relative velocities and friction factors as follows:

Shear stress between the gas phase in #2 and the solids phase in #1.

$$\tau_{gsi} = f_{gi}\frac{1}{2}\rho_{g2}\left(U_{g2} - U_{s1}\right)|U_{g2} - U_{s1}| \tag{30}$$

Shear stress between the solids phase in #2 and the solids phase in #1.

$$\tau_{ssi} = f_{si}\frac{1}{2}\rho_{s}(U_{s2} - U_{s1})|U_{s2} - U_{s1}| \tag{31}$$

Shear stress between the solids phase in #1 and the pipe wall.

$$\tau_{s1} = f_{s1}\frac{1}{2}\rho_{s}U_{s1}^{2} \tag{32}$$

Shear stress between the solids phase in #2 and the pipe wall.

$$\tau_{s2} = f_{s2}\frac{1}{2}\rho_{s}U_{s2}^{2} \tag{33}$$

Shear stress between the gas phase in #1 and the pipe wall.

$$\tau_{g1} = f_{g1}\frac{1}{2}\rho_{g1}U_{g1}^{2} \tag{34}$$

Shear stress between the gas phase in #2 and the pipe wall.

$$\tau_{g2} = f_{g2}\frac{1}{2}\rho_{g2}U_{g2}^{2} \tag{35}$$

where $f_{\alpha k}$ is the wall friction factor for phase α in layer k, and $f_{\alpha i}$ is the layer interface friction factor for phase α in layer #2.

2.2.4.3. Equations of state. In this work, it was assumed that the cross-sectional pressure is uniform. As a consequence, the gas pressure in both layers is the same (i.e., $P \equiv P_1 = P_2$). The gas phase in each layer was assumed to be an ideal gas.

$$P = \rho_{g1}\mathbb{R}T_{g1} = \rho_{g2}\mathbb{R}T_{g2} \tag{36}$$

where $\mathbb{R}$ is the gas constant.

2.2.4.4. Inter-phase drag forces. The inter-phase drag forces, taken into account the in this model, were due to drag between the gas and solids phases. The drag forces per unit length were calculated by multiplying the drag force on a particle by the number of particles per unit length. For solids volume fractions less than 0.2, the drag coefficients were based upon a single particle drag coefficient and modified to take into account the multi-particle effects using the method of Richardson and Zaki (1954). For solids volume fractions greater than 0.2, the drag coefficient was derived from the Ergun (1952) equation.

$$F_{d1} = \frac{3r_{s1}A_1}{4D_p} C_{d1}\rho_{g1}\left(U_{g1} - U_{s1}\right)|U_{g1} - U_{s1}| \tag{37}$$

$$F_{d2} = \frac{3r_{s2}A_2}{4D_p} C_{d2}\rho_{g2}\left(U_{g2} - U_{s2}\right)|U_{g2} - U_{s2}| \tag{38}$$

where C_{dk} is the particle drag coefficient in layer k, and D_p is the mean particle diameter.

2.2.4.5. Heat transfer. The heat transfer between the gas and solids phases in a layer was assumed to be only due to convection.

$$Q_{gk\leftrightarrow sk} = -\frac{6r_{sk}A_k}{D_p} h_{gk\leftrightarrow sk}\left(T_{gk} - T_{sk}\right) \tag{39}$$

where $h_{gk\leftrightarrow sk}$ is the convective heat transfer coefficient between the gas and solids phases in layer k.

The Nusselt number for layer k, Nu_k, was evaluated using:

$$Nu_k = \frac{h_{gk\leftrightarrow sk}D_p}{k_{gk}} = 2.0 + 0.6\, Re_{pk}^{0.5} Pr_{gk}^{0.333} \tag{40}$$

where

k_{gk} is the thermal conductivity of the gas phase in layer k
μ_{gk} is the dynamic viscosity of the gas phase in layer k
Pr_{gk} is the Prandtl number for the gas phase in layer k, $Pr_{gk} = C_{pgk}\mu_{gk}/k_{gk}$.
Re_{pk} is the particle Reynolds number in layer k, $Re_{pk} = \rho_{gk}D_p|U_{gk} - U_{sk}|/\mu_{gk}$

The heat transfer between the layer and the pipe wall is assumed to be governed by convection between the gas phase and the pipe wall.

$$Q_{gk\leftrightarrow wall} = S_k h_{gk}\left(T_{wall} - T_{gk}\right) \tag{41}$$

where h_{gk} is the convective heat transfer coefficient between the gas and the pipe wall in layer k, and T_{wall} is the pipe wall temperature.

The heat transfer in between the layers is assumed to be governed by convection between the gas phase in the top layer and the gas and solids phases in the bottom layer.

$$Q_{g2\leftrightarrow g1} = r_{g1}S_i h_{g2g1}\left(T_{g2} - T_{g1}\right) \tag{42}$$

$$Q_{g2\leftrightarrow s1} = r_{s1}S_i h_{g2s1}\left(T_{g2} - T_{s1}\right) \tag{43}$$

where $h_{g2\alpha1}$ convective heat transfer coefficient between the gas phase and the phase α in layer #1.

The convective heat transfer coefficients, h_{gk}, were calculated from the Nusselt number, Nu_{Dhk}, which was defined as:

$$Nu_{Dhk} = 0.023\, Re_{Dhk}^{0.8} Pr_{gk}^{n} \quad n = \begin{cases} n = 0.3 & \text{for cooling} \\ 0.5 & \text{for heating} \end{cases} \tag{44}$$

The Reynolds number used in this expression is based upon the hydraulic radius, thus:

$$Re_{Dhk} = \frac{\rho_{gk}|U_{gk}|D_{hk}}{\mu_{gk}} = \frac{\rho_{gk}|U_{gk}|}{\mu_{gk}}\frac{4A_k}{S_k}$$

$$Re_{Dhik} = \frac{\rho_{gk}|U_{gk}|D_{hik}}{\mu_{gk}} = \frac{\rho_{gk}|U_{gk}|}{\mu_{gk}}\frac{4A_k}{S_i} \tag{45}$$

for the wall and layer interface, respectively.

2.3. Solution of the balance equations

The above set of equations consist of 12 ordinary differential equations and 12 unknowns, namely: r_{g1}, r_{g2}, h, P, U_{g1}, U_{g2}, U_{s1}, U_{s2}, T_{g1}, T_{g2}, T_{s1}, T_{s2}. Consequently, in principle, the above set of ordinary equations is complete and can be solved. The numerical solution of the above balance equations was obtained using an explicit fifth order Runge–Kutta method (Shampine and Reichelt, 1997). Initial values of the flow conditions were specified at the inlet to the pipe. The solution progressed from the pipe inlet to the outlet.

Using this method, the outlet flow conditions are computed for a given set of inlet flow conditions. In order to simulate the operation of a particular pneumatic conveying system, the inlet conditions may need to be modified in order to, for example, match a specific outlet pressure. Such an algorithm for driving a flow model has been presented by the authors (Mason et al., 1998b).

3. Performance of the model

3.1. Initial conditions

In order to obtain a solution, values for the 12 flow parameters must be specified at the pipe inlet. This poses a problem since, in general, only the following global data are known: pressure and the total gas and solids mass flow rates. The volume fractions of the two phases in each layer and the height of the lower layer are unknown and difficult to measure. The following procedure was developed to specify these initial values:

- The volume fraction of the gas in the lower layer was assumed to be similar to that of the material as poured, i.e. at the poured bulk density.
- The volume fraction of the gas in the upper layer was assumed to be similar to that of a *dilute phase* flow, approximately 1%.
- The ratio of the solids to gas velocity in each layer was taken to be 0.9.

It only remains to select the height of the lower layer; two values were used $0.8D$ and $0.2D$.

Using these assumptions, it is possible to compute the 12 initial flow parameters from the global data.

Fig. 3 shows a comparison between the results obtained for both thick and thin initial lower layers. In both cases, the height of the lower layer achieves an almost constant value. Table 1 shows the two sets of initial conditions and the resulting conditions 15 m downstream. From this, it can be seen that the initial conditions have little effect on the prediction of the fully developed flow region. In fact, the differences between the predicted values for fully developed flow in the gas volume fractions for each layer are less than 1% and the velocity differences are less than 2%.

In this paper, the flow was assumed to be fully developed when the relative velocity between the phases in each layer is virtually constant. This is similar to the definition used by Rose and Duckworth (1969), who stated that "having entered the pipe, the particles are accelerated until a sensibly constant velocity is attained", and assumed that the flow is fully developed at that point.

When comparing the two options for initial layer height, it was found that the thick layer option was more robust. With the thin layer option, the lower layer increases in height due to mass transfer from the upper to lower layer. Thus, the initial mass of solids in the upper layer must be sufficient to form the lower layer. In order to achieve this, the volume fraction of the gas in the upper layer must be reduced, otherwise if it is too high then the model will fail when the gas volume fraction in the upper layer reaches one. Using the thick layer option, there is

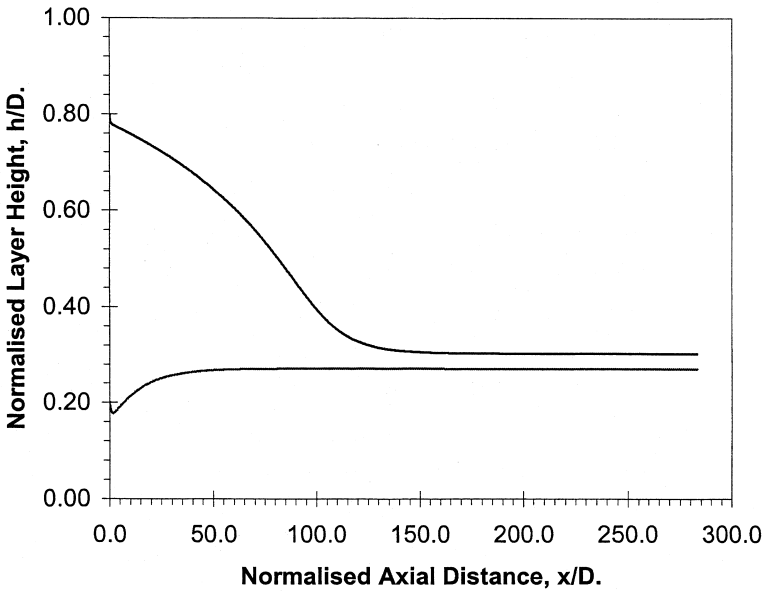

Fig. 3. A comparison of the thick and thin layer options for computing the initial flow parameters.

Table 1
A comparison of inlet and outlet flow parameters when using the thick and thin layer options for computing the initial conditions

Test	r_{g1} (m^3/m^3)	r_{g2} (m^3/m^3)	h (m)	p (Pa_a)	u_{g1} (m/s)	u_{g2} (m/s)	u_{s1} (m/s)	u_{s2} (m/s)
Inlet conditions								
1a	0.650	0.990	0.0424	200000.0	0.807	49.431	0.727	44.488
1b	0.650	0.970	0.0106	200000.0	1.774	8.719	1.596	7.847
Outlet conditions								
1a	0.685	0.979	0.0160	190098.4	1.479	10.353	1.478	10.306
1b	0.689	0.977	0.0143	185950.1	1.454	10.161	1.453	10.116
Δ	0.7%	−0.2%	−10.6%	−2.2%	−1.7%	−1.9%	−1.7%	−1.8%
Total mass flow rate:		Gas = 0.038 kg/s Solids = 1.9 kg/s						
Initial conditions for:		Temperature, $T_{g1} = T_{s1} = T_{g2} = T_{s2} = 300.0$ K Test 1a computed using the thick layer option Test 1b computed using the thin layer option						

no need to do this since the mass transfer is in the opposite direction. As a result, selecting initial conditions using the thick layer option is more straightforward.

A common type of feeder used in pneumatic conveying systems to transport bulk materials in this mode of flow is the *blow tank* (a pressure vessel). An almost full-bore flow of densely packed material may be observed at the discharge from such a feeder when the conveying system is operating in a *dense phase* mode.

3.2. Comparison with experimental data

The experimental data was obtained for the transport of cement. Table 2 shows the properties of the cement used in this experimental programme. The pneumatic conveying

Table 2
Properties of the bulk material used in the experimental work

Material	Ordinary Portland cement
Mean particle size	14 μm
Mass median particle size	21 μm
Particle size range (2.5%/97.5%)	4/37 μm
Particle density	3060 kg/m^3
Poured bulk density	1070 kg/m^3
Tapped bulk density	1500 kg/m^3

system used was comprised of a 0.7 m^3 pressure vessel feeding a horizontal straight pipe 20 m long with an internal diameter of 53 mm. The data collection and flow rate control systems used were similar to those described by Mason and Li (1999). Fig. 4 shows the location of the sensors used in this test programme.

In each test, a constant mass flow rate of gas was supplied to the system. The equilibrium condition of the system is defined as the time period when the overall pressure drop and solids mass flow rate are both approximately constant. Typical sets of data are presented in Fig. 5. Both of these tests show fluctuations in the pressure drop caused mainly by the flow. The unsteady nature of the high concentration flow is shown in Fig. 5b with the *staircase*-like form of the solids mass collected trace.

The average values for all measured quantities are computed for the duration of the equilibrium period. The data used for comparison with the model are presented in Table 3. Also, in this table, the standard deviations computed for each measured value are shown. In subsequent figures, this is used to determine the size of the error bars. A continuous two-layer flow was observed experimentally when the superficial gas velocity was in the range 2–6 m/s. Based upon these observations, values were selected from the test data with an inlet superficial gas velocity of approximately 3 m/s. Three cases were chosen with solids loading ratios of 50–130. Fig. 6 shows a comparison between the model and the experimental data for these test data.

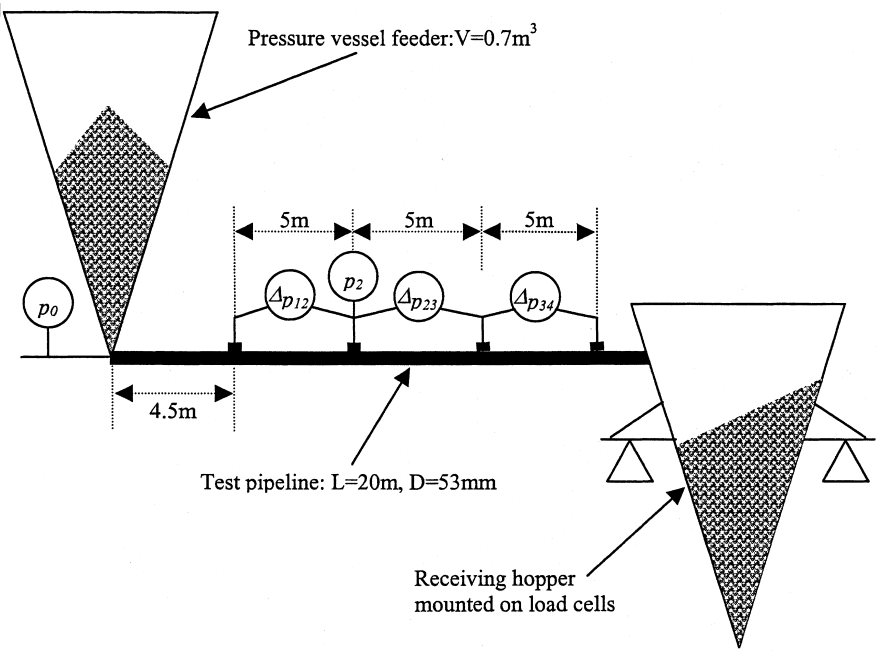

Fig. 4. Location of sensors.

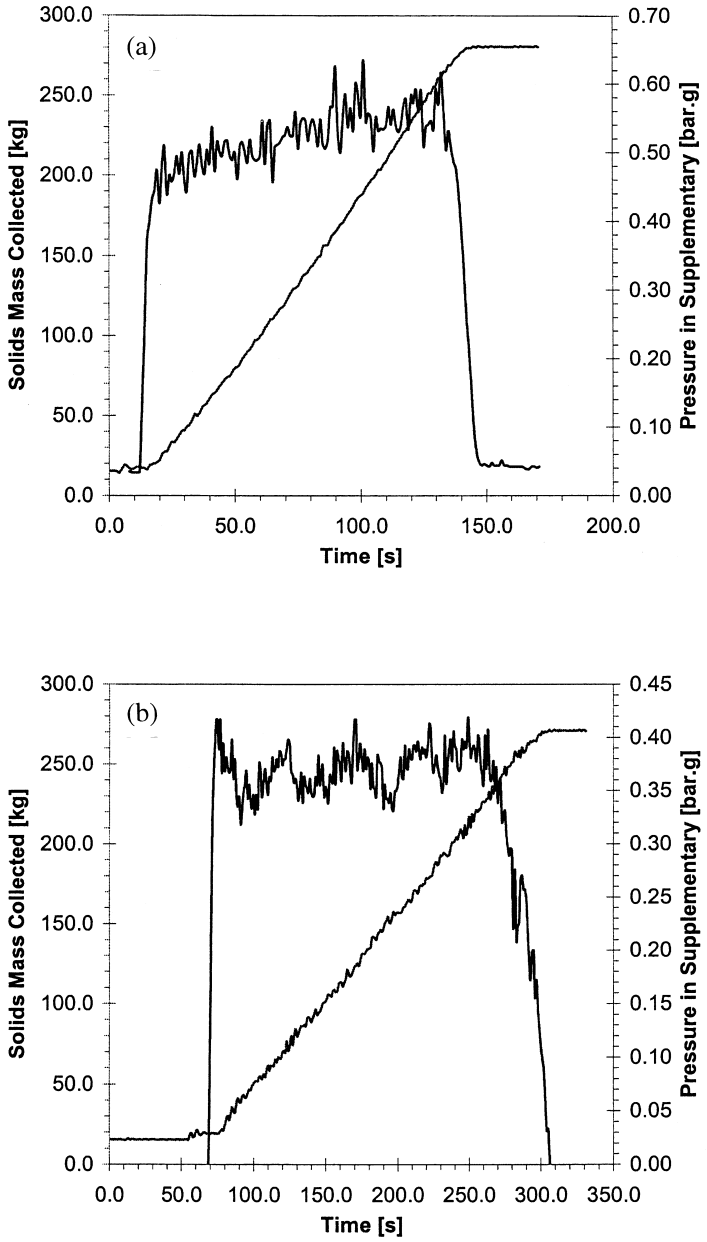

Fig. 5. Typical test data recorded for non-suspension flow of cement. (a) $\dot{m}_g = 0.075$ kg/s, $\dot{m}_s = 2.24$ kg/s, $\Delta p = 0.55$ bar, SLR = 30.0 kg/kg, $U_{gin} = 17.85$ m/s; (b)$\dot{m}_g = 0.011$ kg/s, $\dot{m}_s = 1.09$ kg/s, $\Delta p = 0.37$ bar, SLR = 98.7 kg/kg, $U_{gin} = 3.00$ m/s.

Table 3
Flow conditions used for comparison

Test case	Data	p_0 (Pa_a) $L = 0.0$ m	p_1 (Pa_a) $L = 4.5$ m	p_2 (Pa_a) $L = 9.5$ m	p_3 (Pa_a) $L = 14.5$ m	p_4 (Pa_a) $L = 19.5$ m	$\dot{m}_g$ (kg/s)	$\dot{m}_s$ (kg/s)	SLR[a] (kg/s)
1	Average	128344.1	119230.9	110924.4	106142.3	102507.8	0.0112	0.621	55.5
	Standard deviation	1388.4	2990.5	2771.6	2839.5	2849.7			
2	Average	138266.3	128668.5	118557.9	110503.5	105344.3	0.0110	1.090	98.7
	Standard deviation	1889.4	2261.8	2194.2	2323.2	2354.7			
3	Average	146757.0	132565.8	122160.3	112372.2	105495.6	0.0107	1.371	128.5
	Standard deviation	1723.2	2301.5	2301.5	2371.1	2380.9			
Sensor accuracy		±1500.0	±250.2	±250.0	±250.2	±250.4			

[a] SLR is the solids loading ratio, SLR = $\dot{m}_s\dot{m}_g$..

The pipe may be divided into two regions:

- The developing flow region starting at the solids feed point, which is characterised by a continuously changing pressure gradient;
- The developed flow region, which is characterised by a virtually constant pressure gradient.

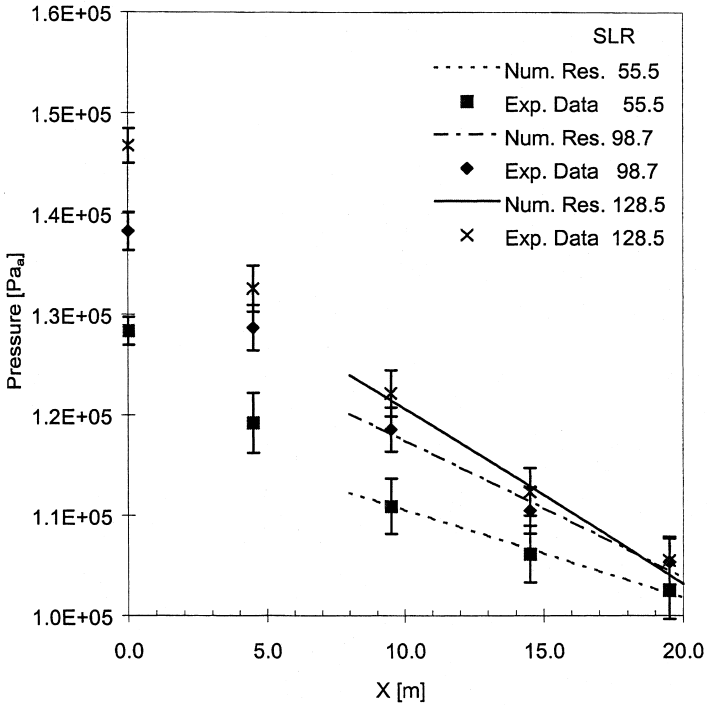

Fig. 6. Comparison of model with experimental data.

In all the experiments, the flow was found to be fully developed from the p_2 sensor location, 9.5 m from the inlet. The selection of the initial conditions poses a major problem since it is not possible to determine all these parameters with the current experimental system. It was previously demonstrated that the initial conditions only have a minor effect on the prediction of the developed flow region. Thus, simulations were made for the developed flow region only, starting from 8 m downstream of the inlet. The predicted pressure profiles correspond very well with the experimental data for all three cases. Although this comparison is not sufficient to validate the model, it does demonstrate the potential of the model.

3.3. Analysis of model behaviour

The model has demonstrated good qualitative agreement with experimental pressure profiles. The following section examines the behaviour of other model's parameters. Fig. 7 shows the height of the lower layer and the gas volume fractions in both layers. The set of three solid lines is for the layer height and relates to the left-hand axis. The height of the lower layer increases from 11 to 30 mm as the solids loading ratio is increased from 55.5 to 128.5, while the solids volume fraction falls from 0.153 to 0.138. In the upper layer the volume fractions are similar with no clear relationship between the volume fraction and solids loading ratio. The differences found between the upper layer, volume fractions are similar to those found from the earlier analysis of the influence of the initial conditions.

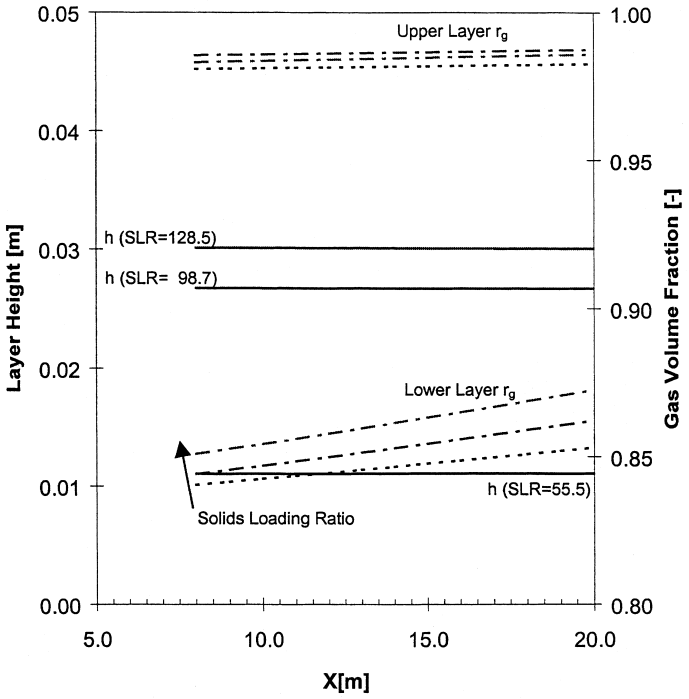

Fig. 7. Predicted layer height and layer volume fractions.

Table 4
Predicted mass flow rates for each layer at the 20 m location[a]

Test	$\dot{m}_{g1}$ (kg/s)	$\dot{m}_{g2}$ (kg/s)	$\dot{m}_{g}$ (kg/s)	$\dot{m}_{s1}$ (kg/s)	$\dot{m}_{s2}$ (kg/s)	$\dot{m}_{s}$ (kg/s)	f_{mg1}	f_{mg2}	f_{ms1}	f_{ms2}
1	0.0003	0.0109	0.0112	0.13	0.49	0.62	3%	97%	21%	79%
2	0.0020	0.0091	0.0110	0.80	0.29	1.09	18%	82%	74%	26%
3	0.0030	0.0077	0.0107	1.10	0.27	1.37	28%	72%	80%	20%

[a] $f_{m\alpha k}$ is the ratio of the mass flow rate of phase α in layer k to the total mass flow rate of phase α..

The variation in the lower layer volume fraction is due to a 10-fold increase in the gas mass flow rate in the layer, which acts to fluidise the layer. The balance of mass flow rates through the pipe cross-section 20 m downstream of the inlet is shown in Table 4. From this table, it can be seen that there is a significant change in the nature of the flow as the solids loading ratio is increased:

- at the lowest value of solids loading ratio, the majority of the solids mass is transferred into the upper layer suspended in the gas;
- at the highest value of solids loading ratio, the majority of the solids mass is transferred into the lower layer.

Fig. 8 shows the variation of gas velocity in the layers for each test case. The upper set of

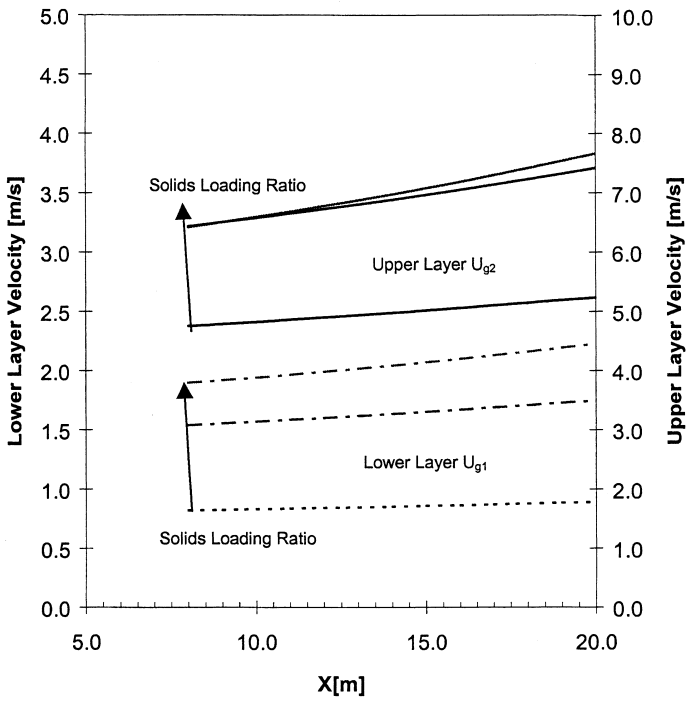

Fig. 8. Predicted gas velocities in each layer.

Table 5
Friction forces for each layer at the 20 m location

Test	Relative wall friction in lower layer	Relative inter-layer friction	Relative wall friction in upper layer	Relative total wall friction	Relative pressure drop (from experiment)
1	6.13	1.00	26.44	1.00	1.00
2	27.72	1.20	23.36	1.57	1.55
3	40.47	1.10	25.09	2.01	1.96
	Friction forces expressed as values relative to the inter-layer friction force for test case 1.			Quantity expressed as values relative to those for test case 1.	

three solid lines is for the upper layer and relates to the right-hand axis. The two cases with higher solids loading ratios show similar velocity profiles in both layers. The third case exhibits a considerably lower velocity in both layers. This supports the previous observation that there is a significant change in the nature of the flow as the solids loading ratio is increased. This change in the flow is linked to the balance of forces acting on the two layers. Table 5 shows a comparison of the predicted friction forces for each test case relative to the smallest force computed. Thus, for case 1, the friction force between the lower layer and the wall is 6.13 times the friction force between the two layers, and that for the upper layer is 26.44 times the inter-layer value.

The relative velocity between the layers is similar for each case and so the inter-layer force grows as the interface area increases. Comparing cases 2 and 3, a small reduction is seen, which is due to a reduction in the interface area since the layer height is greater than 12D in case 3. The upper layer wall friction varies by less than 12% between the three cases. This small change is due to the combined effects of less mass in the layer and a reduction in the surface area of the pipe in contact with the layer. From case 1 to 2, the mass effect dominates and the force decreases; and from case 2 to 3, the area effect dominates and the force increases. The growth of the lower layer as the solids loading ratio is increased from case 1 to 3 results in a seven-fold increase in the wall friction. With the upper layer and inter-layer forces changing by only small amounts, it is the large change in the lower layer friction force that dominates the overall effect. This is also illustrated in Table 5 by comparing the overall friction force with the pressure drop measured experimentally. The total friction force is the sum of the layer wall friction forces. This has been computed as a value relative to that for case 1, thus the force can be seen to double from case 1 to 3. The pressure drop has also been expressed as a value relative to that measured for case 1. The change in the pressure drop and total friction force is similar. This is, as expected, since the pressure drop in the developed flow region is governed by wall friction effects.

4. Conclusion

A two-layer model has been developed to simulate *dense phase* pneumatic transport of fine powders. The model has shown good quantitative agreement with experimentally determined

pressure profiles for fully developed flows in straight horizontal pipes. The behaviour of the model in terms of the variation of layer height, velocity and solids concentration shows good qualitative agreement with the experimental observations. One of the key areas of the investigation has been to determine the influence of the initial conditions on the development of the flow predicted by the model. It has been shown that the initial layer height has little influence on the prediction of the flow conditions in the fully developed region. Although this is sufficient for some applications, accurate prediction of the developing flow region is necessary when modelling complete pipe networks. The performance of the model is promising, and further experimental work is planned to obtain data sufficient to fully validate model. In particular, the nature of the initial flow conditions will be investigated.

References

Bohnet, M., 1965. Experimentelle und theoretische Untersuchugen uber das Absetzen, das Aufwirbeln und den Transport feiner Staubteilchen in pneumatischen Förderleitungen. VDI Forschungsheft 507.

Doron, P., Barnea, D., 1993. A three layer model for solid–liquid flow in horizontal pipe. Int. J. Multiphase Flow 19, 1029–1043.

Ergun, S., 1952. Fluid flow through packed columns. Chem. Eng. Progress 48, 89–94.

Fargette, C., 1998. Bench scale tests for the assessment of pneumatic conveying behaviour of powders. M.Phil. Dissertation, Glasgow Caledonian University, UK.

Hong, J., Tomita, Y., 1993. Analysis of high density gas–solids stratified pipe flow. Int. J. Multiphase Flow 21, 649–665.

Hong, J., Zhu, J.X., 1997. Effect of pipe orientation on dense-phase transport (I): critical angle in inclined upflow. Powder Technol. 91, 115–122.

Jones, M.G., Mason, D.J., Ansell, R.O., Fargette, C., 1998. Development of de-aeration and permeability tests for the assessment of pneumatic conveying capability. In: Proc. 3rd World Congress on Particle Technology, Brighton, UK.

Mason, D.J., 1991. A study of the modes of gas–solids flow in pipelines. Ph.D. Dissertation, University of Greenwich, London, UK.

Mason, D.J., Li, J., 1999. A novel experimental technique for the investigation of gas–solids flow in pipes. In: Proc. 2nd Pneumatic and Hydraulic Conveying, Davos, Switzerland. Powder Technol., in press.

Mason, D.J., Levy, A., Marjanovic, P., 1998a. The influence of bends on the performance of pneumatic conveying systems. Advanced Powder Technol. 9, 197–206.

Mason, D.J., Marjanovic, P., Levy, A., 1998b. A simulation system for pneumatic conveying systems. Powder Technol. 95, 7–14.

Mills, D., 1990. Pneumatic Conveying Design Guide. Butterworths, London.

Muschelknaultz, E., Wojahn, W., 1974. Auslegung pneumatischer förderanlagen. Chemie-Ing. Techn. 46 (Jahrg. Nr 6).

Richardson, J.F., Zaki, W.N., 1954. Sedimentation and fluidization: Part I. Trans. Inst. Chem. Eng. 32, 35–53.

Rose, H.E., Duckworth, R.A., 1969. Transport of solid particles in liquids and gases. The Engineer issues 14, 21, 28 March 1969.

Seville, J.P.K., Tuzun, U., Clift, R., 1997. Processing of Particulate Solids. Chapman & Hall, London.

Shampine, L.F., Reichelt, M.W., 1997. The MATLAB ODE Suite. SIAM Journal on Scientific Computing, 18–1.

Wilson, K.C., 1976. A unified physically based analysis of solid–liquid pipeline flow. Proc. Hydrotransport 4, BHRA. Paper A1, pp. 1–16.

Wilson, K.C., Addie, G.R., Sellgren, A., Clift, R., 1996. Hydraulic Conveying of Solids with Centrifugal Pumps, 2nd ed. Chapman & Hall, London.